**Article**

A blazar in the epoch of reionization

Eduardo Bañados [1] ✉, Emmanuel Momjian[2], Thomas Connor[3],
Silvia Belladitta[1,4], Roberto Decarli [4], Chiara Mazzucchelli[5],
Bram P. Venemans [6], Fabian Walter[1], Feige Wang[7], Zhang-Liang Xie[1],
Aaron J. Barth [8], Anna-Christina Eilers [9], Xiaohui Fan[7], Yana Khusanova [1],
Jan-Torge Schindler[10], Daniel Stern [11], Jinyi Yang [7], Irham Taufik Andika [12,13],
Christopher L. Carilli[2], Emanuele P. Farina [14], Andrew Fabian [15],
Joseph F. Hennawi [6,16], Antonio Pensabene [17] & Sofía Rojas-Ruiz[1,18]

Relativistic jets are thought to play a crucial role in the formation and evolution of massive galaxies and supermassive black holes. Blazars, which are quasars with jets aligned along our line of sight, provide insights into the jetted population and have been observed up to redshifts of $z = 6.1$. Here, we report the discovery and multi-wavelength characterization of the blazar VLASS J041009.05−013919.88 at $z = 7$ (age of the Universe ~750 Myr), which is powered by a ~$7 \times 10^8\ M_\odot$ black hole. The presence of this high-redshift blazar implies a large population of similar but unaligned jetted sources in the early Universe. Our findings suggest two possible scenarios. In one, the jet in J0410−0139 is intrinsically low power but appears highly luminous due to relativistic beaming, suggesting that most ultraviolet-bright quasars at this redshift host jets. Alternatively, if J0410−0139 represents an intrinsically powerful radio source, there should be hundreds to thousands of radio-quiet quasars at $z \approx 7$ with properties like those of J0410−0139, a prediction in tension with observed quasar densities based on their ultraviolet luminosity function. These results support the hypothesis that the rapid growth of black holes in the early Universe may be driven by jet-enhanced or obscured super-Eddington accretion, potentially playing a key role in forming massive black holes during the epoch of reionization.

Relativistic jets are believed to be key drivers in the growth of massive galaxies and supermassive black holes[1], and a few of them have been identified in the first billion years of the Universe[2,3]. We selected the quasar VLASS J041009.05−013919.88 (hereafter J0410−0139) from cross-matching the optical DESI (Dark Energy Spectroscopic Instrument) Legacy Imaging Surveys (DELS)[4] and the 1.4 GHz NRAO (National Radio Astronomy Observatory) VLA (Karl G. Jansky Very Large Array) Sky Survey (NVSS)[5]. We required that the source be undetected in the DELS g- and r-bands (Fig. 1 and Table 1). The NVSS beam was 45″. Thus, the radio emission could arise from several sources. Therefore, we required that the DELS source coincides with an unresolved radio source in the 3 GHz Very Large Array Sky Survey (VLASS)[6]. The VLASS 2.5″ beam unambiguously identified the NVSS radio source with the

DELS source (there were no other radio sources within the NVSS beam). The 3 GHz flux density of J0410−0139 increased by ~35% from the first to the second VLASS epoch (in less than 3 years' observed frame; Fig. 1 and Table 2). This was the first indication that the source might be variable and potentially a blazar.

We confirmed the nature of J0410−0139 on 7 November 2020. A 30 min spectrum recorded by the focal reducer/low dispersion spectrograph 2 (FORS2) at the Very Large Telescope (VLT) in Chile revealed a quasar with a prominent Lyα emission line at $z = 7.0$, within the so-called epoch of reionization when the intergalactic medium was transitioning from neutral to ionized[7,8]. We then obtained near-infrared spectra with the near-infrared echellette spectrometer (NIRES) at the Keck Observatory, the LUCI spectrograph at the Large Binocular Telescope (LBT)
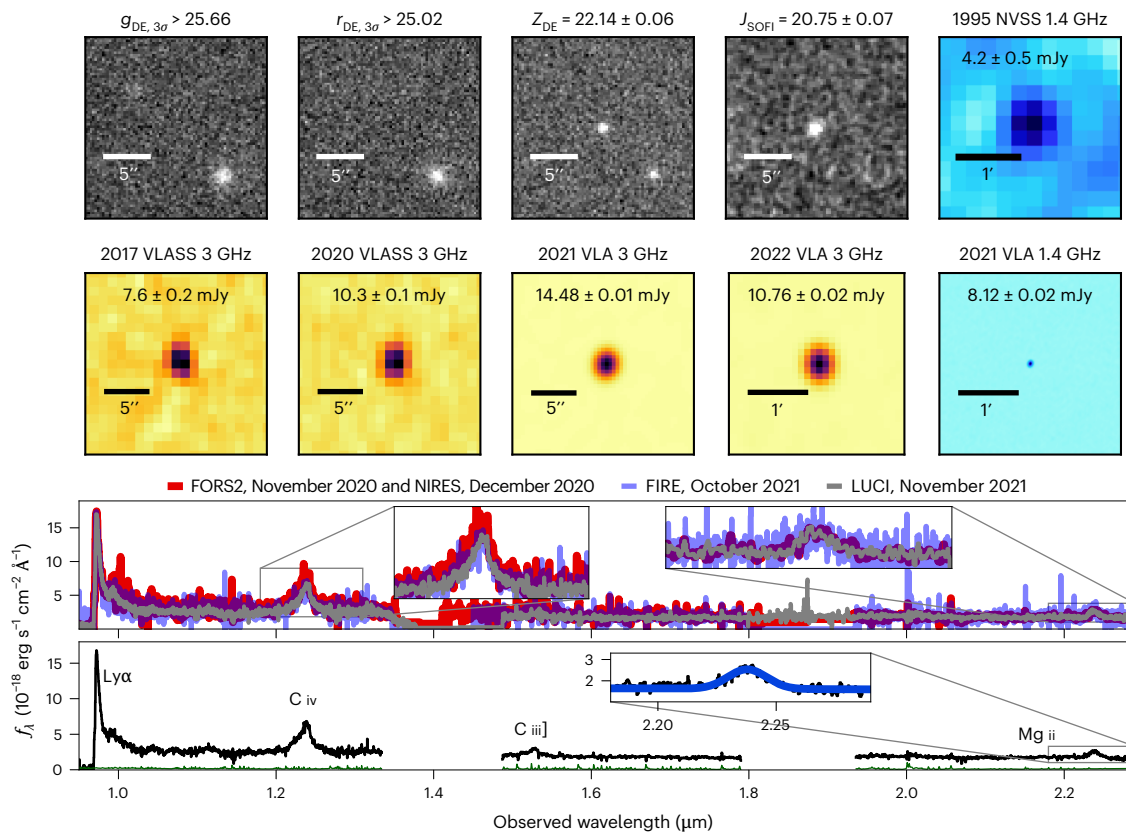
Fig. 1 | Photometry and spectra of the quasar J0410−0139 at z = 7.0. The greyscale postage stamps are optical and near-infrared images. The radio images use different colour maps (3 GHz in orange and 1.4 GHz in light blue). The 1995 NVSS 1.4 and the 2022 VLA 3 GHz images, taken in the most compact VLA configuration, have the lowest resolution. The 2021 VLA 1.4 GHz image, shown at the same size for comparison, confirms that there is a single radio source in the field with strong evidence of variability. The second-to-bottom panel compares spectra from VLT/FORS2, Keck/NIRES, Magellan/FIRE and LBT/LUCI, showing consistent rest-frame UV with no variability in the broad line region or accretion disk. The bottom panel shows the combined spectrum (and the 1σ error in green). Inset, A Gaussian fit to the Mg II line, which was used to estimate the black hole properties (Table 3).

and the folded-port infrared echellette spectrograph (FIRE) mounted on the Magellan Baade Telescope at Las Campanas Observatory (Fig. 1; see Methods for details of the observations). The spectra were taken between November 2020 and November 2021, and the spectral slopes and broad emission line profiles are consistent among them (Fig. 1). Near-infrared follow-up photometry taken between November 2020 and January 2023 is also consistent within 2σ (Table 1). Thus, we found no evidence for variability in the observed near-infrared wavelengths (rest-frame ultraviolet (UV) and optical), implying that there were no strong changes in the accretion disk or broad line region of the quasar. These characteristics are seen in luminous flat-spectrum radio quasars at lower redshifts[9] and are consistent with the flat observed 2.7–5 GHz radio spectrum[10] of J0410−0139 (Fig. 2).

The redshift derived from a Gaussian fit to the Mg II line is $z_{Mg II} = 6.995 \pm 0.001$ (all error bars in this article correspond to 1σ or the central 68% interval of the distribution, unless otherwise stated), but hereafter we use $z_{[C II]} = 6.9964 \pm 0.0005$ as the systemic redshift, measured from observations of the [C II] line by the Atacama Large Millimeter Array and presented in a companion paper[11]. Throughout this paper, we adopt a flat cosmology with a Hubble parameter of $H_0 = 70$ km s^{-1} Mpc^{-1}, and cosmological density parameters $\Omega_M = 0.3$ and $\Omega_\Lambda = 0.7$. In this cosmology, the Universe's age at $z_{[C II]}$ is 751 Myr and 1″ corresponds to 5.23 proper kpc.

We derived a black hole mass of $6.9^{+0.5}_{-0.4} \times 10^8$ times the mass of the Sun ($M_\odot$) from the full-width at half-maximum of the Mg II line and the quasar luminosity at 3,000 Å ($L_{3,000}$; Table 3), following the methods of previous works[12,13]. Adopting a bolometric correction[14] of $L_{bol} = 5.15 L_{3,000}$, the accretion rate or Eddington ratio for J0410−0139 is

Table 1 | Optical and near-infrared photometry of J0410−0139

Survey/Inst.	AB magnitudes	Date
DELS DR10	$g_{DE,3\sigma} > 25.66$	
DELS DR10	$r_{DE,3\sigma} > 25.02$	
DELS DR10	$i_{DE,3\sigma} > 24.45$	
DELS DR10	$Z_{DE} = 22.14 \pm 0.06$	
NTT/SOFI	$J_{SOFI} = 20.75 \pm 0.07$	2020 November 20
NTT/SOFI	$J_{SOFI} = 20.97 \pm 0.12$	2021 July 26
NTT/SOFI	$J_{SOFI} = 20.77 \pm 0.07$	2023 January 4
NTT/SOFI	$H_{SOFI} = 20.85 \pm 0.13$	2020 November 20
NTT/SOFI	$H_{SOFI} = 20.88 \pm 0.07$	2023 January 4
NTT/SOFI	$Ks_{SOFI} = 20.30 \pm 0.08$	2020 November 20
NTT/SOFI	$Ks_{SOFI} = 20.38 \pm 0.10$	2023 January 4
DELS DR10	$W1 = 20.46 \pm 0.08$	
DELS DR10	$W2 = 20.16 \pm 0.15$	

To identify J0410−0139, we used DELS data release 8, but here we report the most recent photometry from DELS data release 10 (DR10). For the DELS DR10 catalogue, the filters are g_{DE}, r_{DE}, i_{DE} and Z_{DE}, corresponding to the filters from the DECam camera. W1 and W2 are the filters onboard the WISE satellite. When the additional subscript $_{3\sigma}$ is included, the quantity reported is a 3-sigma lower limit. For NTT/SOFI the filters are J_{SOFI}, H_{SOFI} and Ks_{SOFI}.

$L_{bol}/L_{Edd} = 1.22 \pm 0.08$. These properties are comparable to what is observed in other quasars at a similar cosmic time but without evidence of powerful relativistic jets[13].

Table 2 | Radio observations of J0410−0139

Frequency (GHz)	Flux density (mJy)	Date	Image beam (position angle)	Reference
0.856	5.09±0.30	2021 December 18	23.1″×11.8″ (−61°)	FLASH[68]
0.888	5.64±0.90	2019 April 26	25.0″×25.0″ (0°)	RACS[69]
0.888	5.42±0.97	2020 June 20	15.1″×12.4″ (85°)	VAST[70]
0.888	5.10±0.8	2021 July 21	13.6″×11.9″ (79°)	VAST[70]
1.37	7.89±1.62	2021 July 28	9.4″×7.6″ (88°)	VAST[70]
1.37	11.99±1.84	2021 September 20	12.9″×7.1″ (67°)	VAST[70]
1.37	5.83±1.5	2021 November 18	10.6″×7.8″ (81°)	VAST[70]
1.40	4.20±0.50	1995	45.0″×45.0″ (0°)	NVSS[5]
1.5	8.12±0.02	2021 September 25	4.26″×3.45″ (−18°)	VLA/21B-087
1.5	4.46±0.04	2021 November 17	0.0143″×0.0059″ (1°)	VLBA/21B-190
1.5	9.21±0.17	2022 August 06	40.5″×34.5″ (3°)	VLA/21B-087
3.0	7.60±0.20	2017 October 1	2.8″×2.1″ (16°)	VLASS1.1 (ref. 6)
3.0	10.29±0.14	2020 July 19	2.8″×2.1″ (−1°)	VLASS2.1 (ref. 6)
3.0	14.48±0.01	2021 September 25	2.16″×1.83″ (−9°)	VLA/21B-087
3.0	10.63±0.02	2022 August 6	23.13″×19.53″ (2°)	VLA/21B-087
3.0	10.10±0.15	2023 March 8	2.8″×2.1″ (1°)	VLASS3.1 (ref. 6)
5.0	15.70±0.01	2021 September 25	1.37″×1.02″ (−8°)	VLA/21B-087
5.0	11.05±0.01	2022 August 6	16.0″×11.6″ (−0°)	VLA/21B-087
6.0	14.88±0.01	2021 September 25	1.23″×0.89″ (−2°)	VLA/21B-087
6.0	10.66±0.01	2022 August 6	13.0″×9.0″ (7°)	VLA/21B-087
7.0	14.04±0.01	2021 September 25	1.13″×0.79″ (2°)	VLA/21B-087
7.0	10.28±0.01	2022 August 6	11.5″×8.0″ (10°)	VLA/21B-087
8.74	9.45±0.01	2022 August 6	9.0″×0.58″ (−4°)	VLA/21B-087
8.87	12.79±0.01	2021 September 25	0.77″×6.9″ (3°)	VLA/21B-087
10.0	12.01±0.005	2021 September 25	0.69″×0.52″ (−4°)	VLA/21B-087
10.0	8.87±0.06	2022 August 6	0.77″×0.58″ (−4°)	VLA/21B-087
10.19	8.79±0.01	2022 August 6	7.8″×5.9″ (11°)	VLA/21B-087
10.7	11.54±0.01	2021 September 25	0.64″×0.49″ (−4°)	VLA/21B-087

The peak flux densities for QL VLASS1.1 were corrected by 15%, and for VLASS2.1 and VLASS3.1 by 8% (Methods). FLASH, First Large Absorption Survey in H ɪ; RACS, Rapid ASKAP Continuum Survey; VAST, Variables and Slow Transients (VAST) pilot survey.

Observational signatures of a blazar or a relativistic jet pointing close to our line of sight include[15]: (1) strong variable radio emission, (2) flat or peaked core-dominated radio spectrum, (3) compact or core-jet radio morphology, (4) flat X-ray photon index ($\Gamma_X < 1.8$) and (5) flat rest-frame 10 keV to 2,500 Å flux ratio ($\widetilde{\alpha}_{OX} > -1.36$). Below we show that J0410−0139 satisfies all these criteria.

Figure 2a shows the full spectral energy distributions (SEDs) of J0410−0139 and low-redshift blazars with similar radio and X-ray luminosities[16]. We compiled all existing archival radio observations of J0410−0139 (Table 1) and obtained quasi-simultaneous VLA observations on 25 September 2021 and on 6 August 2022 from 1 to 12 GHz, corresponding to rest-frame 8 to 96 GHz (Methods). The measured flux densities differed from all archival observations, confirming a highly variable radio SED, as shown in Fig. 2b. The quasi-simultaneous 2021 VLA observations reveal a turnover at rest-frame ~40 GHz, making J0410−0139 a gigahertz peaked radio source that resembles other blazars[17]. The observations are indicative of a young jet or a blazar flaring event[18,19]. The 2022 radio SED shows a flatter spectrum with a less pronounced peak. Figure 2c shows the light curves at observed frequencies of 1.4 and 3.0 GHz, spanning 3.4 years and 8 months in the rest frame of the quasar, respectively. They are incompatible with the expectations of a young radio source in adiabatic expansion[20,21]. The flux density exhibited a change by a factor of 3 over 14 days in

the rest frame of the quasar. Such variability and change of the radio spectral shape are similar or more extreme than that of blazars at lower redshifts[22,23].

On 17 November 2021, we obtained 14.3 × 5.9 mas (75 × 37 pc) resolution Very Long Baseline Array (VLBA) observations at 1.5 GHz (Methods and Fig. 3). The VLBA image reveals a dominant, marginally resolved source with a flux density of 4.46 ± 0.04 mJy. This flux density is consistent with the NVSS measurement observed more than 15 years earlier but is fainter than most contemporaneous data (Fig. 2c). At present, it is unclear whether the 'missing' flux of the VLBA observations is due to variability or that we might be resolving extended emission over a few parsecs. We obtained X-ray observations of J0410−0139 with XMM-Newton on 4 August 2022 and with Chandra over six observations from 21 November 2022 to 21 December 2022 (Methods and Fig. 3). When fitted with a single model, the derived X-ray properties are a luminosity of $L_{2\text{-}10\,\text{keV}} = 3.2^{+0.8}_{-0.7} \times 10^{45}$ erg s^{-1}, a photon index of $\Gamma_X = 1.47^{+0.19}_{-0.17}$, and $\widetilde{\alpha}_{OX} = -1.25 \pm 0.02$. Besides satisfying the blazar classification[15], $\Gamma_X < 1.8$ and $\widetilde{\alpha}_{OX} > -1.36$, note that non-blazar quasars typically have $\Gamma_X \approx 1.9$ and that there is a strong indication that the $z > 6$ quasars are softer[24] with an average $\Gamma_X = 2.4 \pm 0.1$.

Based on a simple geometrical consideration[2,25], the existence of this blazar implies that there should be many more intrinsically similar jetted sources (for example, with similar black hole masses and
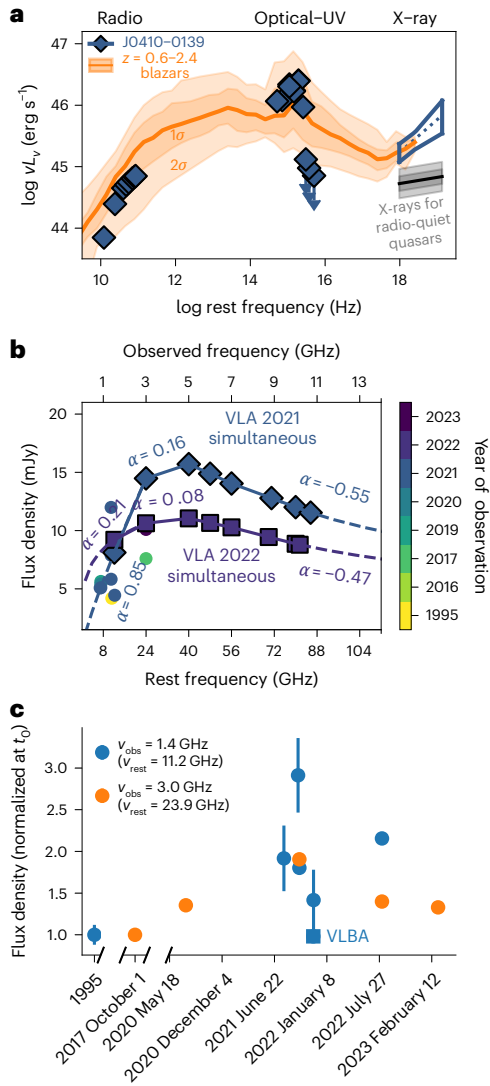
Fig. 2 | SED and radio light curves of J0410−0139. a, Rest-frame SED from radio to X-rays, showing only the simultaneous VLA 2021 observations. Strong absorption in the UV (shown as 3σ upper limits) is due to absorption from the neutral intergalactic medium at $z \approx 7$. The X-ray uncertainties consider 2σ variation in the X-ray photon index and flux densities. The shaded orange regions span the 1σ and 2σ SED distributions for low-redshift flat-spectrum radio blazars[16] with similar X-ray luminosities. The orange curve marks the median SED. The grey shading represents the 1σ and 2σ expected X-ray luminosity for a radio-quiet quasar with the same $L_{2,500}$ (ref. 71). **b**, Radio SED with data points colour-coded by year (Table 1). The quasar shows strong variability across radio frequencies. Diamonds (squares) represent quasi-simultaneous VLA 2021 (2022) observations, within 15 min in the rest frame. Dashed lines are power-law extrapolations from these measurements. **c**, Observed 1.4 and 3.0 GHz radio light curves (ν_{obs}) (11.2 and 23.9 GHz rest-frame radio light curves, ν_{rest}). Data points are normalized to the initial flux density for each frequency, with 1σ error bars shown. The 1.4 GHz values were corrected using spectral index values of $\alpha = 0.85$ (pre-2022) and $\alpha = 0.21$ (post-2022).

Table 3 | Derived properties of J0410−0139

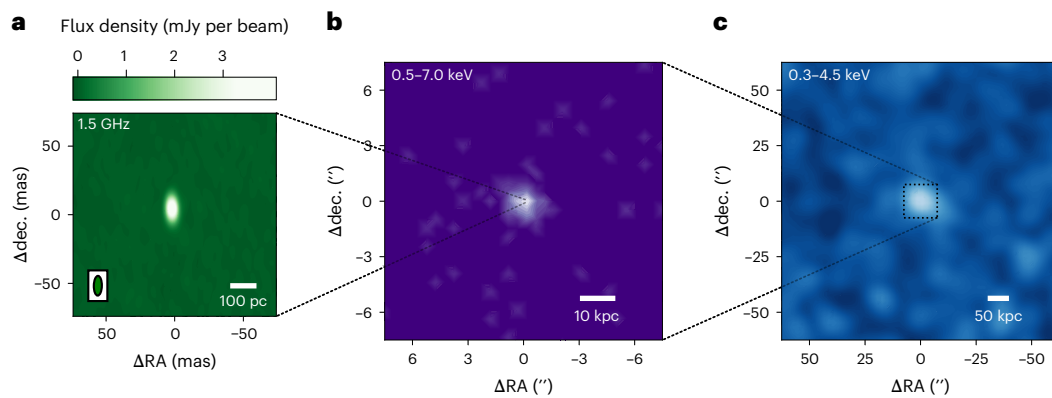| Quantity	Value	Units
z_{MgII}	6.995±0.001	
$z_{[CII]}$	6.9964±0.0005	
$m_{1,450}$	21.33±0.08	AB mag
$M_{1,450}$	−25.60±0.08	AB mag
$L_{2,500}$	(2.0±0.1)×10^{46}	erg s^{-1}
$L_{3,000}$	(2.1±0.1)×10^{46}	erg s^{-1}
$L_{4,400}$	(2.5±0.2)×10^{46}	erg s^{-1}
L_{5GHz}(2021)	(13.590±0.003)×10^{42}	erg s^{-1}
$R_{2,500}$(2021)	165±11	
$R_{4,400}$(2021)	74±5	
L_{5GHz}(2022)	(27.210±0.006)×10^{42}	erg s^{-1}
$R_{2,500}$(2022)	331±22	
$R_{4,400}$(2022)	148±9	
$FWHM_{MgII}$	2562$^{+90}_{-80}$	km s^{-1}
M_{BH}	6.9$^{+0.5}_{-0.4}$ × 10^8	$M_\odot$
L_{bol}	(1.096±0.005)×10^{47}	erg s^{-1}
L_{bol}/L_{Edd}	1.22±0.08	
$L_{2-10 keV}$	3.2$^{+0.8}_{-0.7}$ × 10^{45}	erg s^{-1}
Γ_X	1.47$^{+0.19}_{-0.17}$	
α_{OX}	−1.46 ± 0.07	
$\tilde{\alpha}_{OX}$	−1.25 ± 0.02	

$L_{2,500}$, $L_{3,000}$ and $L_{4,400}$ were measured from the best-fitting power-law model to the combined spectrum. The uncertainties were dominated by the $Ks_{SOFI} = 20.30 \pm 0.08$ magnitude used to absolute flux-calibrate the spectrum. For L_{5GHz}(2021), $R_{2,500}$(2021), $R_{4,400}$(2021), L_{5GHz}(2022), $R_{2,500}$(2022) and $R_{4,400}$(2022) the rest-frame 5 GHz luminosity and radio loudness were found using the radio measurements from 25 September 2021 and 6 August 2022 (Table 1 and Fig. 2a). For α_{OX}, $\alpha_{OX} \equiv \log(L_{\nu_X}/L_{\nu_{UV}})/\log(\nu_X/\nu_{UV})$, where L_ν is the monochromatic luminosity. In this work, and in keeping with standard practice, we evaluated ν_{UV} at 2,500 Å and ν_x at 2 keV (α_{OX}) and 10 keV ($\tilde{\alpha}_{OX}$). z_{MgII}, redshift based on the Mg II emission line; $z_{[CII]}$, redshift based on the [C II] emission line; $m_{1,450}$, apparent magnitude at rest-frame 1,450 Å; $M_{1,450}$, absolute magnitude at rest-frame 1,450 Å; $L_{2,500}$, luminosity at rest-frame 2,500 Å; $L_{3,000}$, luminosity at rest-frame 3,000 Å; $L_{4,400}$, luminosity at rest-frame 4,400 Å; L_{5GHz}(2021), luminosity at rest-frame 5 GHz measured in 2021; $R_{2,500}$(2021), radio loudness defined as the ratio between the flux densities at rest-frame 5 GHz and 2,500 Å, with the 5 GHz flux density measured in 2021; $R_{4,400}$(2021), radio loudness defined as the ratio between the flux densities at rest-frame 5 GHz and 4,400 Å, with the 5 GHz flux density measured in 2021; L_{5GHz}(2022), luminosity at rest-frame 5 GHz measured in 2022; $R_{2,500}$(2022), radio loudness defined as the ratio between the flux densities at rest-frame 5 GHz and 2,500 Å, with the 5 GHz flux density measured in 2022; $R_{4,400}$(2022), radio loudness defined as the ratio between the flux densities at rest-frame 5 GHz and 4,400 Å, with the 5 GHz flux density measured in 2022; $FWHM_{MgII}$, full width at half maximum of the Mg II broad emission line; M_{BH}, mass of the black hole; L_{bol}, bolometric luminosity; L_{Edd}, Eddington luminosity; L_{bol}/L_{Edd}, Eddington ratio; $L_{2-10 keV}$, X-ray luminosity at 2–10 keV; Γ_X, X-ray photon index.

$$= N_{jetted} \left[1 - \cos\left(\frac{1}{\Gamma}\right) \right] \quad (3)$$

where Γ is the bulk Lorentz factor of the emitting plasma, and Ω is the solid angle subtended by the jet. Using the first two terms of the Taylor series for $\cos(1/\Gamma)$, the total number of jetted sources given one blazar is $N_{jetted} \simeq 2\Gamma^2$. Bulk Lorentz factors for blazars[26,27] range from 1 to 40. If Γ is close to 1, that could suggest a truly unique source. The distribution of bulk Lorentz factors for low-redshift blazars[26,28] peaks between $\Gamma = 5$ and 15, and at $z > 4$, $\Gamma \approx 5$ provides a good match to observational constraints[29]. Assuming Γ is in the range 4–15, we would expect about 30–450 jetted sources like J0410−0139 at $z \approx 7$. Thus far, there are only two other spectroscopically confirmed jetted quasars[3,30] at a comparable redshift ($z \approx 6.8$), implying that many $z \approx 7$ radio sources are yet to be identified.

Quasars are observationally classified as radio loud if their radio-loudness parameter[3,31]—the ratio of the rest-frame 5 GHz

redshifts) pointing elsewhere, including optically obscured quasars. More specifically, the number of blazars with a viewing angle $\theta \le 1/\Gamma$ (for $\Gamma \gg 1$) is related to the total jetted population, N_{jetted}, as:

$$N(\theta \le 1/\Gamma) = N_{jetted} \times \frac{2\Omega}{4\pi} \quad (1)$$

$$= N_{jetted} \int_0^{1/\Gamma} \sin(\theta) \, d\theta \quad (2)$$

Fig. 3 | High-resolution 1.5 GHz radio and X-ray observations of J0410−0139. **a**, VLBA 1.5 GHz image with a beam size of 14.3 × 5.9 mas (75 × 37 pc). The source is marginally resolved with a size <3 mas (<16 pc). **b**, Chandra/ACIS 0.5–7.0 keV image. **c**, XMM/EPIC 0.3–4.5 keV image. J0410−0139 is unresolved in the XMM

and Chandra images and is the strongest X-ray source in the field. The VLBA and X-ray images reveal a single compact dominant source, supporting the blazar interpretation. dec., declination, RA, right ascension.

(radio) flux density ($f_{5\,GHz}$) to the 4,400 Å (optical) flux density ($f_{4,400\,A}$) or 2,500 Å (UV) flux density ($f_{2,500\,A}$)−is greater than 10. With the caveat that this source shows strong radio variability, we estimated its radio loudness by extrapolating the radio slopes measured from our two quasi-simultaneous 2021 and 2022 VLA observations to rest-frame 5 GHz; that is, with $\alpha = 0.85$ and $\alpha = 0.21$, respectively (in the convention $f_\nu \propto \nu^\alpha$; Fig. 2a). This results in radio-loudness parameters $R_{2,500} = f_{5\,GHz}/f_{2,500\,A} = 165$ and $R_{4,400} = f_{5\,GHz}/f_{4,400\,A} = 74$ in 2021 and $R_{2,500} = 331$ and $R_{4,400} = 148$ in 2022 (Table 3).

However, it is plausible that J0410−0139 has an intrinsically low-power, weak jet and that the observed radio loudness is due only to relativistic Doppler boosting. An enhancement of only 7.4 (14.8) would have made this quasar radio quiet in 2021 (2022). The observed flux density is enhanced as $f_{\nu,obs} = \delta^{(3-\alpha)} \times f_{\nu,int}$, where α is the radio spectral index and δ is the relativistic Doppler factor $\delta = [\Gamma(1 - \beta\cos(\theta))]^{-1}$ and $\beta = \sqrt{1 - (1/\Gamma^2)}$, and $f_{\nu,int}$ is the intrinsic flux density. Figure 4a is a Doppler enhancement diagram for J0410−0139, which shows a substantial chance that we see boosted flux (even reaching factors of ∼10^{3-4}).

If the intrinsic luminosity of this radio jet is much lower than observed, the argument for $2\Gamma^2$ similar sources still holds. However, the expected number of jetted sources approaches the total number of UV-bright quasars derived from the $z \approx 7$ quasar UV luminosity function (Fig. 4b). The implication is that a large fraction of UV-bright quasars must have a relativistic radio jet even if they are classified as radio quiet. This aligns with the fact that some of the most massive quasars known at high redshift, although classified as radio quiet, show evidence of relativistic radio jets[32]. At low redshift, the origin of the radio emission for radio-quiet quasars is still debated, but there exist examples of relativistic jets powered by an active galactic nucleus that do not meet the observational criteria for classification as radio loud[33,34]. Note that the expected contribution from star formation to radio emission is less than four orders of magnitude[35] of the observed radio luminosity of J0410−0139. Confirmation that a large fraction of the highest-redshift quasars are jetted could have profound implications, as relativistic jets could affect the interstellar medium of their host galaxies[36] and enhance the growth of supermassive black holes[37,38].

The radio-loud fraction of quasars is constant[39,40] at ∼10% from $z < 1$ to $z \approx 6$. Thus, if J0410−0139 is intrinsically radio loud ($R_{4,400} > 10$), then that implies that there should be ∼10 times more radio-quiet quasars at similar redshifts. This strongly conflicts with the numbers expected from the quasar UV luminosity function[41], as shown in Fig. 4b. As the number predicted from the detection of a blazar also includes obscured quasars, a way to reconcile the results is that most black hole growth must happen in an obscured phase. Such obscured growth is predicted by some theoretical models[42,43], and it is observationally supported

by the obscured $z = 6.8$ quasar recently discovered in a small region of the sky[30] and by obscured but intrinsically luminous candidate active galactic nuclei uncovered by the James Webb Space Telescope[44,45].

The presence of J0410−0139 implies that jet-enhanced[37,46] or obscured, sustained super-Eddington[42] accretion can play a key role in the growth of supermassive black holes at early times. Both scenarios ease the tension regarding the existence of supermassive black holes in the early Universe, leaving the collapse of dense star clusters and the remnants of population III stars as still viable options as initial 'seeds'.

Methods
VLASS flux densities
For the identification and radio characterization of J0410−0139, we used peak flux densities from the first data products of the VLASS survey[6]: the VLASS quick-look (QL) images. The QL images have some known systematic offsets of their flux densities (https://science.nrao. edu/vlass/data-access/vlass-epoch-1-quick-look-users-guide). In practice, the peak flux densities of QL VLASS1.1 data are low by ~15%, whereas for VLASS2.1 and VLASS3.1, they are low by ~8%. We have taken these factors into account in the values reported in Table 1.

During the revision of this paper, the VLASS2.1 single-epoch (SE) continuum image of J0410−0139 was released. The SE images are intended to be the VLASS reference data products and supersede the QL images (https://science.nrao.edu/vlass/vlass-se-continuum-users-guide.) Therefore, we give the SE VLASS2.1 measurements in Table 1. The difference between the SE and QL flux densities is 0.49 ± 0.24 mJy.

Data and data reduction
Near-infrared imaging. We obtained two epochs of J_{SOFI}, H_{SOFI} and Ks_{SOFI} imaging with SOFI[47] at the New Technology Telescope (NTT) in La Silla on 20 November 2020 and 4 January 2023. Another epoch of J_{SOFI} was obtained only on 26 July 2021. The data were bias-subtracted, flat-fielded, sky-subtracted and stacked. The photometric zero points were calibrated using stars from the 2MASS[48] survey. The NTT/SOFI photometry is reported in Table 1. The photometry from 2020 and 2023 are consistent within the uncertainties, whereas the J_{SOFI} photometry from 2021 was slightly fainter by only 0.2 mag, but consistent within 2σ.

Spectroscopy. We obtained a 30 min spectrum on 7 November 2020 with VLT/FORS2[49]. The FORS2 spectrum detected a strong Lyα line and a sharp Lyman break, confirming the quasar nature of J0410−0139. On 26 December 2020, we obtained a 1.2 h Keck/NIRES[50] spectrum, which revealed strong C IV and Mg II broad emission lines. We observed J0410−0139 on 23 September 2021 and 15 October 2021 for a total of 6 h

a

b
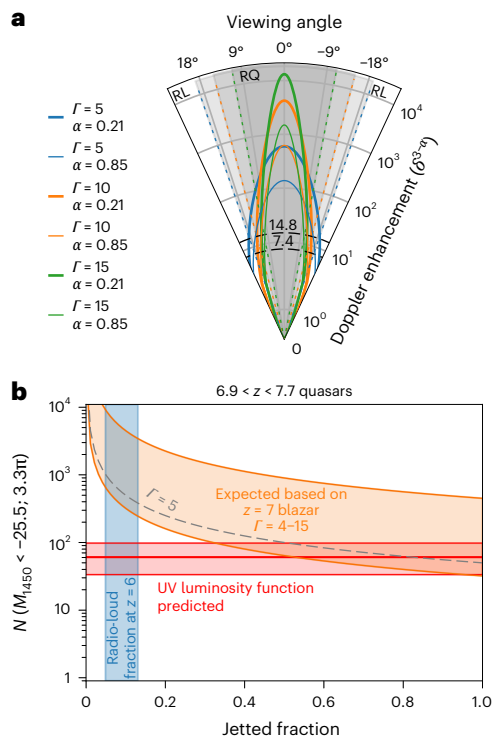
Fig. 4 | Doppler enhancement and tension with the expected number of quasars at z ≈ 7. a, Doppler enhancement diagram for different bulk Lorentz factors (Γ) and radio spectral indices ($\alpha = 0.85$ for 2021 and $\alpha = 0.21$ for 2022). J0410−0139 is classified as radio loud with $R_{4400} = 74$ (148), but its jet may be intrinsically weak depending on relativistic Doppler enhancement. The dashed lines indicate a Doppler enhancement of 7.4 (14.8), which is critical for reclassifying the quasar as radio quiet in 2021 (2022). The shaded region represents viewing angles where J0410−0139 would be intrinsically weak for the respective Γ. For larger angles, the jet power would be substantial, thus maintaining its classification as radio loud. **b**, Expected number of $6.9 < z < 7.7$ quasars brighter than $M_{1450} = -25.5$ over 3.3π of the sky (covered by NVSS and VLASS) as a function of the fraction of quasars with relativistic jets. The thick horizontal red line represents the expected number based on the $z \approx 7$ quasar UV luminosity function, and the shaded region indicates the 1σ uncertainty[41]. The existence of this blazar suggests that there are ~$2\Gamma^2$ quasars with similar properties but misaligned jets. The orange region shows the expected number of comparable quasars assuming typical low-redshift blazar values[27] of $\Gamma = 4$–15 as a function of the jetted fraction (f_{jetted}): $N_{total} = N_{jetted}/f_{jetted} = 2\Gamma^2/f_{jetted}$. The dashed line represents an average $\Gamma = 5$, consistent with observations[29] at $z > 4$. This estimate is in tension with the UV luminosity function. The shaded blue region shows the measured radio-loud fraction[40] at $z = 6$. If the jet from J0410−0139 is weak but appears radio loud due to beaming, the tension decreases if the jetted fraction of UV-bright quasar exceeds 70%. Conversely, if the jet from J0410−0139 is powerful and the radio-loud fraction remains 10% at $z \approx 7$, the total number of quasars would exceed expectations by at least an order of magnitude. RL, radio loud; RQ, radio quiet.

with the Magellan/FIRE spectrograph[51] in echelle mode. On 23 October 2021 and 12 November 2021, we obtained fraternal mode spectroscopy with the LUCI spectrograph[52] at the LBT, where *zJ* and *HK* observations were carried out simultaneously. The November observations were taken under good weather conditions, whereas bad weather in October severely affected the data. We discarded all individual frames with a signal-to-noise ratio <0.1, which eliminated all the October *HK* data. The total effective exposure times for the *zJ* and *HK* spectra were 5 and 3.5 h, respectively.

All the spectra were reduced with the Python spectroscopic data reduction pipeline (PypeIt)[53]. The LBT/LUCI and Magellan/FIRE data were absolute flux-calibrated to match the $Ks_{SOFI} = 20.30$ photometry. The VLT/FORS2 and Keck/NIRES spectra were scaled to match the

flux-calibrated Magellan/FIRE spectral continuum. Figure 1 shows the individual and combined spectra. It reveals strong broad emission lines typical of blazars that are not BL Lacertae sources[9,54]. The continuum slope and profile of the broad emission lines are consistent across all the different spectra. Stable broad line regions have also been seen in low-redshift blazars in multi-epoch spectroscopic campaigns[55,56].

VLA. To characterize the radio SED of the quasar J0410−0139, we carried out observations with the VLA of the NRAO in its B configuration (maximum baseline of 11.1 km) on 25 September 2021. The frequency range of the VLA observations spanned 1 to 12 GHz using the L- (1–2 GHz), S- (2–4 GHz), C- (4–8 GHz) and X- (8–12 GHz) band receivers. The total on-source time was ~20 min in the L- and S-bands and ~22 min in the C- and X-bands. The source J0542+4951 (3C 147) was observed as the flux density scale calibrator and band-pass calibrator, and the source J0423−0120 was observed to calibrate the complex gains. The L- and S-band observations used the 8 bit samplers of the VLA, whereas the C- and X-bands used the 3 bit samplers. The wideband interferometric digital architecture (WIDAR) correlator was configured to use the default NRAO wideband set-ups that deliver 16 × 64 MHz sub-bands for the L-band, 16 × 128 MHz sub-bands for the S-band and 32 × 128 MHz sub-bands for both the C- and X-bands. Data editing, calibration, deconvolution and imaging were carried out using the Common Astronomy Software Applications (CASA)[57] package. Self-calibration in phase only for the L- and C- bands and in both phase and amplitude for the S- and X-bands was also performed on the target source to improve the dynamic range and image fidelity. Self-calibration for the L-, S- and C-bands was carried out in CASA. The X-band data were self-calibrated in phase using CASA, whereas the amplitude self-calibration required the use of the Astronomical Image Processing System (AIPS)[58] to properly constrain the amplitude gain values.

Another epoch of VLA L-, S-, C- and X-band observations on the target source were carried out with the D configuration (maximum baseline of 1 km) on 6 August 2022. The set-up and the data reduction were like those used for the B-configuration observations. The flagging of radio-frequency interference resulted in slightly different effective central frequencies between the 2021 and 2022 data (Table 1).

The final images were all made in CASA using a weighting scheme intermediate between uniform and natural (robust = 0.4 in CASA tclean) and using the multi-terms multi-frequency synthesis (MTMFS) algorithm with two terms (nterms = 2 in CASA tclean). The latter allowed us to model both the total intensity and the variations of the spectral index in the sky. These final images were centred at 1.5 GHz (L-band data), 3 GHz (S-band data), 5 and 7 GHz (C-band data), and 8.9 and 10.7 GHz (X-band data). The synthesized beam sizes at full-width at half-maximum are reported in Table 1.

A two-dimensional Gaussian fit of the source at all these frequencies and epochs revealed a pure point source. The measured flux densities are listed in Table 1.

VLBA. J0410−0139 was observed with the VLBA of the NRAO at 1.5 GHz (L-band) on 17 November 2021. Eight 32 MHz sub-band pairs were recorded at each station using the ROACH digital back end and the polyphase filterbank (PFB) digital signal-processing algorithm, for both right- and left-handed circular polarizations, and sampled at 2 bits. The total bandwidth was 256 MHz, centred at 1.54 GHz. The total observing time in the L-band was 6 h, with 4.1 h on target.

The VLBA observations used nodding-style phase-referencing using the calibrator source J0408−0122, which was 0.54° from the target. The phase-referencing cycle time was 5 min: 4 min on the target and 1 min on the calibrator. The uncertainty in the calibrator position was 0.13 mas in right ascension and 0.27 mas in declination. As employed in these observations, phase-referencing preserves absolute astrometric positions[59] to better than 0.01″. The observations also included the calibrator source 3C 84, which was used as a fringe finder

and band-pass calibrator. Amplitudes were calibrated using measurements of the antenna gain and the system temperature of each station. The data were correlated with the VLBA DiFX correlator[60] in Socorro, NM, with 1 s correlator integration time. Data reduction and analysis were performed in AIPS following standard data reduction procedures for very-long-baseline interferometry. The phase-reference source was self-calibrated, and the solutions were applied on the target field. Deconvolution and imaging of the target were performed using natural weighting (Robust = 5 in AIPS task IMAGR).

Figure 3 shows a VLBA 1.5 GHz (12 GHz rest frame) image of J0410−0139 at an angular resolution of 14.3 × 5.9 mas (75 × 37 pc) with a position angle of 1°. The r.m.s. noise in the image is 20 μJy per beam. This image shows a dominant, marginally resolved source with a flux density of 4.46 ± 0.04 mJy and a size <3 mas (<16 pc). The derived intrinsic brightness temperature lower limit is 2×10^9 K.

X-ray observations. We observed J0410−0139 with XMM-Newton on 4 August 2022 for 55 ks using the European Photon Imaging Camera (EPIC)[61,62]. Observations were reduced with the XMM Science Analysis Software (SAS) v.19.0.0, and after filtering for periods of high background, we had effective exposure times of 28.2 ks (MOS1), 28.6 ks (MOS2) and 13.6 ks (pn). A combined image of these observations is shown in Fig. 3. There are no other notable X-ray sources in the immediate vicinity of the quasar. We used a circular extraction region of radius 20″ centred on the quasar for spectral analysis. The resultant spectra were binned to a minimum of 5 counts per bin.

Additionally, we observed J0410−0139 with Chandra in six observations totalling 132 ks, starting 25 November 2022 and finishing 21 December 2022. J0410−0139 was positioned on the ACIS-S3 chip, and data were collected with the very faint telemetry format. Chandra observations were reduced and processed with the software Chandra Interactive Analysis of Observations (CIAO) v.4.15 (ref. 63). We used a circle of radius 3″ for spectral extraction. As before, we binned the combined spectrum to a minimum of 5 counts per bin. The variability between the two observation sets was below the statistical uncertainties.

We performed the spectral analysis with XSPEC[64] to minimize the C-statistic[65,66]. We modelled the X-ray emission as a power law with a Galactic absorption component[67] of 6.99×10^{20} cm^{-2}. When jointly fitting both observations with the same model, the best fit (C/degrees of freedom = 218.54/205) was found for a power-law index of $\Gamma_X = 1.47^{+0.19}_{-0.17}$ and 1 keV flux density $S_{1\,keV} = 1.90^{+0.31}_{-0.30}$ nJy, corresponding to an intrinsic X-ray luminosity of $L_{2\text{-}10\,keV} = 3.2^{+0.8}_{-0.7} \times 10^{45}$ erg s^{-1} and a modelled flux of $f_{0.5\text{-}7.0\,keV} = 1.71^{+0.22}_{-0.19} \times 10^{-14}$ erg s^{-1} cm^{-2}. From this fit and the rest-frame UV luminosity reported above, we found $\alpha_{OX} = -1.46 \pm 0.07$ and $\tilde{\alpha}_{OX} = -1.25 \pm 0.02$ (see Table 3 for their definitions). Note that the Γ_X and $\tilde{\alpha}$ values for J0410−0139 are consistent with what is expected for blazars[15] and in contrast to most of the X-ray properties of other $z > 6$ quasars[24].

Data availability
The data used in this study can be accessed from the observatories' public archives or the surveys' websites. The datasets generated and analysed during this study are available from the corresponding author upon reasonable request.

References

1. Blandford, R., Meier, D. & Readhead, A. Relativistic jets from active galactic nuclei. *Annu. Rev. Astron. Astrophys.* **57**, 467–509 (2019).
2. Belladitta, S. et al. The first blazar observed at z > 6. *Astron. Astrophys.* **635**, L7 (2020).
3. Bañados, E. et al. The discovery of a highly accreting, radio-loud quasar at z=6.82. *Astrophys. J.* **909**, 80 (2021).
4. Dey, A. et al. Overview of the DESI Legacy Imaging Surveys. *Astron. J.* **157**, 168 (2019).
5. Condon, J. J. et al. The NRAO VLA Sky Survey. *Astron. J.* **115**, 1693–1716 (1998).
6. Lacy, M. et al. The Karl G. Jansky Very Large Array Sky Survey (VLASS). Science case and survey design. *Publ. Astron. Soc. Pac.* **132**, 035001 (2020).
7. Davies, F. B. et al. Quantitative constraints on the reionization history from the IGM damping wing signature in two quasars at z > 7. *Astrophys. J.* **864**, 142 (2018).
8. Wang, F. et al. A significantly neutral intergalactic medium around the luminous z = 7 quasar J0252-0503. *Astrophys. J.* **896**, 23 (2020).
9. Ghisellini, G. & Tavecchio, F. Fermi/LAT broad emission line blazars. *Mon. Not. R. Astron. Soc.* **448**, 1060–1077 (2015).
10. Urry, C. M. & Padovani, P. Unified schemes for radio-loud active galactic nuclei. *Publ. Astron. Soc. Pac.* **107**, 803 (1995).
11. Bañados, E. et al. Far-infrared and [C II] observations of a z=7 blazar. Preprint at arxiv.org/abs/2408.12299 (2024).
12. Vestergaard, M. & Osmer, P. S. Mass functions of the active black holes in distant quasars from the Large Bright Quasar Survey, the Bright Quasar Survey, and the Color-selected Sample of the SDSS Fall Equatorial Stripe. *Astrophys. J.* **699**, 800–816 (2009).
13. Fan, X., Bañados, E. & Simcoe, R. A. Quasars and the intergalactic medium at cosmic dawn. *Annu. Rev. Astron. Astrophys.* **61**, 373–426 (2023).
14. Richards, G. T. et al. Spectral energy distributions and multiwavelength selection of type 1 quasars. *Astrophys. J. Suppl. Ser.* **166**, 470–497 (2006).
15. Ighina, L. et al. X-ray properties of z > 4 blazars. *Mon. Not. R. Astron. Soc.* **489**, 2732–2745 (2019).
16. Massaro, E. et al. The 5th edition of the Roma-BZCAT. A short presentation. *Astrophys. Space Sci.* **357**, 75 (2015).
17. Coppejans, R. et al. Radio spectra of bright compact sources at z > 4.5. *Mon. Not. R. Astron. Soc.* **467**, 2039–2060 (2017).
18. Tinti, S., Dallacasa, D., de Zotti, G., Celotti, A. & Stanghellini, C. High frequency peakers: young radio sources or flaring blazars? *Astron. Astrophys.* **432**, 31–43 (2005).
19. O'Dea, C. P. & Saikia, D. J. Compact steep-spectrum and peaked-spectrum radio sources. *Astron. Astrophys. Rev.* **29**, 3 (2021).
20. Orienti, M. & Dallacasa, D. Variability and parsec-scale radio structure of candidate compact symmetric objects. *Mon. Not. R. Astron. Soc.* **499**, 1340–1355 (2020).
21. Nyland, K. et al. Quasars that have transitioned from radio-quiet to radio-loud on decadal timescales revealed by VLASS and FIRST. *Astrophys. J.* **905**, 74 (2020).
22. Mufakharov, T. et al. Flux-density measurements of the high-redshift blazar PSO J047.4478+27.2992 at 4.7 and 8.2 GHz with RATAN-600. *Mon. Not. R. Astron. Soc.* **503**, 4662–4666 (2021).
23. Komossa, S. et al. MOMO. VI. Multifrequency radio variability of the blazar OJ 287 from 2015 to 2022, absence of predicted 2021 precursor-flare activity, and a new binary interpretation of the 2016/2017 Outburst. *Astrophys. J.* **944**, 177 (2023).
24. Zappacosta, L. et al. Hyperluminous quasars at the epoch of reionization (HYPERION): a new regime for the X-ray nuclear properties of the first quasars. *Astron. Astrophys.* **678**, A201 (2023).
25. Volonteri, M., Haardt, F., Ghisellini, G. & Della Ceca, R. Blazars in the early Universe. *Mon. Not. R. Astron. Soc.* **416**, 216–224 (2011).
26. Hovatta, T., Valtaoja, E., Tornikoski, M. & Lähteenmäki, A. Doppler factors, Lorentz factors and viewing angles for quasars, BL Lacertae objects and radio galaxies. *Astron. Astrophys.* **494**, 527–537 (2009).
27. Saikia, P., Körding, E. & Falcke, H. Lorentz factor distribution of blazars from the optical fundamental plane of black hole activity. *Mon. Not. R. Astron. Soc.* **461**, 297–303 (2016).

28. Hovatta, T. & Lindfors, E. Relativistic jets of blazars. *New Astron. Rev.* **87**, 101541 (2019).

29. Diana, A. et al. The evolution of the heaviest supermassive black holes in jetted AGNs. *Mon. Not. R. Astron. Soc.* **511**, 5436–5447 (2022).

30. Endsley, R. et al. ALMA confirmation of an obscured hyperluminous radio-loud AGN at $z=6.853$ associated with a dusty starburst in the 1.5 deg^2 COSMOS field. *Mon. Not. R. Astron. Soc.* **520**, 4609–4620 (2023).

31. Kellermann, K. I., Sramek, R., Schmidt, M., Shaffer, D. B. & Green, R. VLA observations of objects in the Palomar Bright Quasar Survey. *Astron. J.* **98**, 1195–1207 (1989).

32. Sbarrato, T., Ghisellini, G., Giovannini, G. & Giroletti, M. Jetted radio-quiet quasars at $z>5$. *Astron. Astrophys.* **655**, A95 (2021).

33. Macfarlane, C. et al. The radio loudness of SDSS quasars from the LOFAR Two-metre Sky Survey: ubiquitous jet activity and constraints on star formation. *Mon. Not. R. Astron. Soc.* **506**, 5888–5907 (2021).

34. Wang, A. et al. VLBI observations of a sample of Palomar-Green quasars. I. Parsec-scale morphology. *Mon. Not. R. Astron. Soc.* **518**, 39–53 (2023).

35. Ceraj, L. et al. The VLA-COSMOS 3 GHz Large Project: star formation properties and radio luminosity functions of AGN with moderate-to-high radiative luminosities out to $z\sim6$. *Astron. Astrophys.* **620**, A192 (2018).

36. Venturi, G. et al. MAGNUM survey: compact jets causing large turmoil in galaxies. Enhanced line widths perpendicular to radio jets as tracers of jet-ISM interaction. *Astron. Astrophys.* **648**, A17 (2021).

37. Jolley, E. J. D. & Kuncic, Z. Jet-enhanced accretion growth of supermassive black holes. *Mon. Not. R. Astron. Soc.* **386**, 989–994 (2008).

38. Ghisellini, G., Haardt, F., Della Ceca, R., Volonteri, M. & Sbarrato, T. The role of relativistic jets in the heaviest and most active supermassive black holes at high redshift. *Mon. Not. R. Astron. Soc.* **432**, 2818–2823 (2013).

39. Ivezić, Ž. et al. Optical and radio properties of extragalactic sources observed by the FIRST Survey and the Sloan Digital Sky Survey. *Astron. J.* **124**, 2364–2400 (2002).

40. Bañados, E. et al. Constraining the radio-loud fraction of quasars at $z>5.5$. *Astrophys. J.* **804**, 118 (2015).

41. Matsuoka, Y. et al. Quasar luminosity function at $z=7$. *Astrophys. J.* **949**, L42 (2023).

42. Johnson, J. L. & Upton Sanderbeck, P. R. A simple condition for sustained super-Eddington black hole growth. *Astrophys. J.* **934**, 58 (2022).

43. Satyavolu, S., Kulkarni, G., Keating, L. C. & Haehnelt, M. G. The need for obscured supermassive black hole growth to explain quasar proximity zones in the epoch of reionization. *Mon. Not. R. Astron. Soc.* **521**, 3108–3126 (2023).

44. Labbe, I. et al. UNCOVER: candidate red active galactic nuclei at $3<z<7$ with JWST and ALMA. Preprint at arxiv.org/abs/2306.07320 (2023).

45. Lambrides, E. et al. Uncovering a massive $z\sim7.7$ galaxy hosting a heavily obscured radio-loud active galactic nucleus candidate in COSMOS-Web. *Astrophys. J.* **961**, L25 (2024).

46. Connor, T., Bañados, E., Cappelluti, N. & Foord, A. Uncovering the first AGN jets with AXIS. *Universe* **10**, 227 (2024).

47. Moorwood, A., Cuby, J.-G. & Lidman, C. SOFI sees first light at the NTT. *Messenger* **91**, 9–13 (1998).

48. Skrutskie, M. F. et al. The Two Micron All Sky Survey (2MASS). *Astron. J.* **131**, 1163–1183 (2006).

49. Appenzeller, I. & Rupprecht, G. FORS - the focal reducer for the VLT. *Messenger* **67**, 18–21 (1992).

50. Wilson, J. C. et al. Mass producing an efficient NIR spectrograph. In *Proc. SPIE Conference Series, Ground-based Instrumentation for Astronomy* Vol. 5492 (eds Moorwood, A. F. M. & Iye, M.) 1295–1305 (SPIE, 2004).

51. Simcoe, R. A. et al. FIRE: a facility class near-infrared echelle spectrometer for the Magellan Telescopes. *Publ. Astron. Soc. Pac.* **125**, 270–286 (2013).

52. Buschkamp, P. et al. LUCI in the sky: performance and lessons learned in the first two years of near-infrared multi-object spectroscopy at the LBT. In *Proc. SPIE Conference Series, Ground-based and Airborne Instrumentation for Astronomy IV* Vol. 8446 (eds McLean, I. S. et al.) 84465L (SPIE, 2012).

53. Prochaska, J. et al. PypeIt: the Python spectroscopic data reduction pipeline. *J. Open Source Softw.* **5**, 2308 (2020).

54. Sbarrato, T. et al. Blazar candidates beyond redshift 4 observed with GROND. *Mon. Not. R. Astron. Soc.* **433**, 2182–2193 (2013).

55. Carnerero, M. I. et al. Multiwavelength behaviour of the blazar OJ 248 from radio to γ-rays. *Mon. Not. R. Astron. Soc.* **450**, 2677–2691 (2015).

56. Raiteri, C. M. et al. Unveiling the monster heart: unbeamed properties of blazar 4C 71.07. *Mon. Not. R. Astron. Soc.* **493**, 2793–2804 (2020).

57. McMullin, J. P., Waters, B., Schiebel, D., Young, W. & Golap, K. CASA Architecture and Applications. In *Proc. SPIE Conference Series, Astronomical Data Analysis Software and Systems XVI* Vol. 376 (eds Shaw, R. A. et al.) 127 (SPIE, 2007).

58. Greisen, E. W. in *Information Handling in Astronomy – Historical Vistas* Vol. 285 of *Astrophysics and Space Science Library* (ed. Heck, A.) 109 (2003).

59. Fomalont, E. B. in *Synthesis Imaging in Radio Astronomy II* Vol. 180 (eds Taylor, G. B. et al.) 301 (ASP, 1999).

60. Deller, A. T. et al. DiFX-2: a more flexible, efficient, robust, and powerful software correlator. *Publ. Astron. Soc. Pac.* **123**, 275 (2011).

61. Strüder, L. et al. The European photon imaging camera on XMM-Newton: the pn-CCD camera. *Astron. Astrophys.* **365**, L18–L26 (2001).

62. Turner, M. J. L. et al. The European photon imaging camera on XMM-Newton: the MOS cameras. *Astron. Astrophys.* **365**, L27–L35 (2001).

63. Fruscione, A. et al. CIAO: Chandra's data analysis system. In *Proc. SPIE Conference Series, Observatory Operations: Strategies, Processes, and Systems* Vol. 6270 (eds Silva, D. R. & Doxsey, R. E.) 62701V (SPIE, 2006).

64. Arnaud, K. A. in *Astronomical Data Analysis Software and Systems V* Vol. 101 (eds Jacoby, G. H. & Barnes, J.) 17 (ASP, 1996).

65. Cash, W. Parameter estimation in astronomy through application of the likelihood ratio. *Astrophys. J.* **228**, 939–947 (1979).

66. Wachter, K., Leach, R. & Kellogg, E. Parameter estimation in X-ray astronomy using maximum likelihood. *Astrophys. J.* **230**, 274–287 (1979).

67. HI4PI Collaboration. et al. HI4PI: a full-sky H ɪ survey based on EBHIS and GASS. *Astron. Astrophys.* **594**, A116 (2016).

68. Allison, J. R. et al. The First Large Absorption Survey in H ɪ (FLASH). I. Science goals and survey design. *Publ. Astron. Soc. Aust.* **39**, e010 (2022).

69. Hale, C. L. et al. The Rapid ASKAP Continuum Survey Paper. II. First Stokes I source catalogue data release. *Publ. Astron. Soc. Aust.* **38**, e058 (2021).

70. Murphy, T. et al. The ASKAP Variables and Slow Transients (VAST) pilot survey. *Publ. Astron. Soc. Aust.* **38**, e054 (2021).

71. Lusso, E. & Risaliti, G. The tight relation between X-ray and ultraviolet luminosity of quasars. *Astrophys. J.* **819**, 154 (2016).

Acknowledgements

Author contributions

Competing interests

The authors declare no competing interests.

Additional information

Correspondence and requests for materials should be addressed to Eduardo Bañados.

Peer review information *Nature Astronomy* thanks Ryan Hickox and the other, anonymous, reviewer(s) for their contribution to the peer review of this work.

Reprints and permissions information is available at www.nature.com/reprints.

Publisher's note Springer Nature remains neutral with regard to jurisdictional claims in published maps and institutional affiliations.

[1]Max-Planck-Institut für Astronomie, Heidelberg, Germany. [2]National Radio Astronomy Observatory, Pete V. Domenici Science Operations Center, Socorro, NM, USA. [3]Center for Astrophysics | Harvard & Smithsonian, Cambridge, MA, USA. [4]INAF – Osservatorio di Astrofisica e Scienza dello Spazio, Bologna, Italy. [5]Instituto de Estudios Astrofísicos, Facultad de Ingeniería y Ciencias, Universidad Diego Portales, Santiago, Chile. [6]Leiden Observatory, Leiden University, Leiden, The Netherlands. [7]Steward Observatory, University of Arizona, Tucson, AZ, USA. [8]Department of Physics and Astronomy, University of California, Irvine, CA, USA. [9]MIT Kavli Institute for Astrophysics and Space Research, Cambridge, MA, USA. [10]Hamburger Sternwarte, Universität Hamburg, Hamburg, Germany. [11]Jet Propulsion Laboratory, California Institute of Technology, Pasadena, CA, USA. [12]Technical University of Munich, TUM School of Natural Sciences, Department of Physics, Garching, Germany. [13]Max-Planck-Institut für Astrophysik, Garching, Germany. [14]Gemini Observatory, NSF's NOIRLab, Hilo, HI, USA. [15]Institute of Astronomy, Cambridge, UK. [16]Department of Physics, University of California, Santa Barbara, CA, USA. [17]Dipartimento di Fisica 'G. Occhialini', Università degli Studi di Milano-Bicocca, Milan, Italy. [18]Department of Physics and Astronomy, University of California, Los Angeles, Los Angeles, CA, USA. ✉e-mail: banados@mpia.de